Article

Colloidal Silicon-Germanium Nanorod Heterostructures

Xiaotang Lu, María de la Mata, Jordi Arbiol, and Brian A. Korgel

Just Accepted

Colloidal Silicon-Germanium Nanorod Heterostructures

Xiaotang Lu,[†] María de la Mata,[‡,⊥] Jordi Arbiol,[‡,§] Brian A. Korgel*[†]

[†] McKetta Department of Chemical Engineering and Texas Materials Institute, The University of Texas at Austin, Austin, Texas 78712-1062, USA

[‡] Catalan Institute of Nanoscience and Nanotechnology (ICN2), CSIC and BIST, Campus UAB, Bellaterra, 08193 Barcelona, Catalonia, Spain

[§] ICREA, Pg. Lluís Companys 23, 08010 Barcelona, Catalonia, Spain

[⊥] Departamento de Ciencia de los Materiales e I.M. y Q.I., Facultad de Ciencias, Universidad de Cádiz, Puerto Real, 11510, Spain

*Corresponding author: korgel@che.utexas.edu

ABSTRACT

Colloidal nanorods with axial silicon (Si) and germanium (Ge) heterojunction segments were produced by solution-liquid-solid (SLS) growth using tin (Sn) as a seed metal and trisilane and diphenylgermane as Si and Ge reactants. The low solubility of Si and Ge in Sn helps to generate abrupt Si-Ge heterojunction interfaces. To control the composition of the nanorods, it was also necessary to limit an undesired side reaction between the Ge reaction byproduct tetraphenylgermane and trisilane. High resolution transmission electron microscopy (HRTEM) reveals that the Si-Ge interfaces are epitaxial, which gives rise to a significant amount of bond strain resulting in interfacial misfit dislocations that nucleate stacking faults in the nanorods.

INTRODUCTION

Colloidal nanostructures can be made with a wide variety of shapes and composition.[1-4] Heterostructures represent one interesting class of these materials—that is, those with an abrupt change in composition internally.[5] Core-shell heterostructures were the first nanocrystals of this type to be made,[6-8] and since then nanorods and nanowires, as well as branched nanocrystals like tetrapods, have been demonstrated with axial heterojunctions.[9-11] Various approaches have been used to make nanorods and nanowires with axial heterojunctions, including facet-selective epitaxial deposition,[12] ion exchange[13] and metal-seeded growth processes like vapor-liquid-solid (VLS)[14] and solution-liquid-solid (SLS) methods.[10,11] With the ability to tune the electronic band structure by modulating composition or doping lengthwise, nanorods and nanowires with axial heterojunctions have been explored in a variety of applications, including electronic devices,[15-18] photovoltaics,[19-21] photocatalytic systems,[22,23] batteries[24,25] and photonics.[26,27]

VLS and analogous techniques in solvents like SLS and supercritical fluid-liquid-solid (SFLS)[28] growth provide general routes to making nanorods and nanowires that do not rely on intrinsic characteristics of the material to induce uniaxial crystal growth.[29,30] For axial heterojunctions with abrupt transitions in composition, seed metals with a low solubility for the semiconductor are typically required,[31-34] although some researchers have found ways to carefully control reactant addition to overcome the retention of semiconductor species in the seed metal in some instances.[35] If the metal seed retains a significant amount of the semiconductor as the composition of reactants is switched, the resulting compositional interface in the nanowire becomes diffuse.[32,33] Significant efforts have been made to identify suitable metals to seed the growth of nanowires with axial heterojunctions.[31-34] Low melting metals have been found to generally work well for SLS growth of semiconductor nanowires, such as Bi,[36-39] In[40] and Sn[41-43]

and are strong candidates for nanowires with axial heterojunctions. The commonly used gold seeds for example retain significant Si and Ge during growth—with a eutectic composed of nearly 20at% Si—makes it less desirable seed metal for heterojunction nanowires.[34] Nanowires with abrupt axial heterojunctions of Si and Ge have been synthesized using VLS approaches with Al,[31] Au-Ga alloys,[32,33] and Sn[34] seeds. We have been developing solution-based SLS routes to make Si and Ge nanorods with thinner diameters than those typically obtained by VLS—closer to what is needed for quantum confinement at room temperature.[43,44] These methods have used Sn nanoparticles as seeds and have yielded Si nanorods that have exhibited high efficiency carrier multiplication[45] and room temperature photoluminescence.[43]

Here, we show that it is possible to use Sn-seeded SLS growth to produce nanorods with axial Si-Ge heterojunctions. We find that Sn works well as a seed metal for producing abrupt interfaces, as Geaney, et al.[34] showed using their VLS process, but that side reactions can occur in solution that can spoil the compositional profile of the nanorods if not controlled. In the case of VLS growth, it is usually unwanted sidewall deposition that can occur as reactants are switched.[46,47] In the SLS process, sidewall deposition is generally not a major problem, but we find that the diphyenlygermane (DPG) reaction byproduct of tetraphenylgermane that accumulates in the system over time can react with trisilane and prevent Si supply to the growing nanorods. We discuss to what extent this problem can be overcome by manipulating the growth process. A detailed examination of the structure and composition of the nanorod heterojunctions was carried out using transmission electron microscopy (TEM) coupled with electron energy loss spectroscopy (EELS). Because of the difference in lattice constants for Si and Ge, strain is expected across the heterojunction, which can affect the electronic and structural properties of heterojunctions.[48,49] With the help of geometric phase analyses (GPA), the strain at the epitaxial

Si-Ge interface, the presence of misfit dislocations and associated stacking faults, were observed and examined.

EXPERIMENTAL DETAILS:

Materials. Bis[bis(trimethylsilyl)amino]tin(II) (Sn(hmds)$_2$, Aldrich), diphenylgermane (DPG, Gelest), trisilane (Si$_3$H$_8$, Voltaix), octadecane (99%, Aldrich), monophenylsilane (MPS, Gelest), squalane (>95%, Aldrich), poly(vinylpyrrolidinone)-hexadecane (PVP-HDE) copolymer (Ganex V-216, ISP Technologies, Inc.) were used without further purification. Solutions of squalane and PVP-HDE dissolved in octadecane (33% w/w) were degassed under vacuum at 80°C for 45 min and stored in a nitrogen-filled glovebox prior to use.

Nanorod Synthesis. Si-Ge heterojunction nanorods were synthesized using a modification of procedures developed for Si and Ge nanorods (the experimental setup is illustrated in Figure S6).[44] The entire operation is conducted inside a nitrogen-filled glovebox. For the growth of short Ge-Si nanorods, 10 mL of squalane was heated to 360°C under N$_2$ flow in a flat bottom flask attached to the Schlenk line. Separately, a precursor solution of 1 mL of PVP-HDE octadecane solution, 20 μL of Sn(hmds)$_2$, 95 μL of DPG and 45 μL of MPS was prepared in a 3 mL vial, which turned dark brown after mixing, indicating the formation of Sn nanoparticles. MPS was added to facilitate the decomposition of DPG.[50] The precursor solution was then drawn into a syringe equipped with a 6" needle. Prior to injection, the stopcock valve was closed. The mixture was quickly injected through the septum into the hot squalane to initiate the growth of the Ge segment. During this growth period, a second precursor solution of 200 μL of squalane and 42 μL of trisilane was prepared and loaded to another clean syringe. After 5 min following the first injection, the second precursor was injected into the flask. After another 5

min, the heating mantle was removed to allow the flask cool down to room temperature. The stopcock valve was kept closed through the whole reaction to reduce evaporation. (Caution: trisilane is relatively volatile, highly flammable and pyrophoric and must be safely handled.)

Long Ge-Si nanorods were grown by increasing the amount of trisilane to 63 μL in the second injection. In the growth of the Ge-Si-Si nanorods, the first and the second injections were the same as in the reaction of the short Ge-Si nanorods; in the third injection, the precursor solution was made of 200 μL of squalane and 42 μL of trisilane and the growth lasted for 5 min. In the growth of the Ge-Si-Ge nanorods, the first and the second injections were the same as in the reaction of the long Ge-Si nanorods; in the third injection, the precursor solution was made of 200 μL of squalane, 95 μL of DPG and 45 μL of MPS.

The crude reaction product of the nanorod dispersion was diluted with 10 mL of toluene and transferred to a centrifuge tube. About 15 mL of ethanol was then added slowly and the solution was centrifuged at 10000 rpm for 10 min to isolate the product. The supernatant was discarded. The precipitate was redispersed in toluene and washed by repeating the precipitation procedure for three times. The final product was dispersed in chloroform.

Transmission electron microscopy (TEM). Low-resolution TEM images were obtained on a FEI Tecnai Spirit Bio Twin operated at 80 kV. High-resolution transmission electron microscopy (HRTEM) and annular dark-field scanning transmission electron microscopy (ADF-STEM) combined with electron energy loss spectroscopy (EELS) analyses were obtained on a FEI Tecnai F20 microscope operated at 200 kV. The instrument is equipped with a field emission gun, achieving a lateral resolution below 0.14 nm and a Gatan Imaging Filter (GIF) Quantum SE 963 fitted with a 2k x 2k CCD camera, suitable for EELS measurements. TEM

5

samples were prepared by drop-casting 5 μL of diluted nanorods dispersion onto a 200 mesh copper carbon film TEM grid (Electron Microscopy Science).

RESULTS AND DISCUSSON

Synthesis of Si-Ge heterostructure nanorods and strain mapping across the heterojunction. In previous work,[43,44] we showed that Sn nanoparticles are an excellent catalyst for the colloidal growth of both Si and Ge nanorods: the low eutectic temperature of Sn-Si $(231.9^{\circ}C)$[49] and Sn-Ge $(231.1^{\circ}C)$[51] significantly decreases the high crystallization temperatures of Si and Ge and enables the solution-based synthesis. Importantly for this work, the very low solubility of Si and Ge in Sn also makes it a good choice to seed nanorods with Si-Ge heterojunctions. The eutectic points in the Sn-Si and Sn-Ge phase diagrams are located at the Si compositions of only 5×10^{-5} at.%[52] and 2.6×10^{-1} at.%,[51] respectively. The length of the transition region of a heterojunction is proportional to the concentration of the initially-grown species in the liquid seed droplet—a higher solubility results in a more diffuse interface and vice versa.[31,34] Geaney, *et al.*[34] showed that the interface across Si-Ge heterojunctions in Sn-seeded VLS-grown nanowires was 1-2 atomic planes thick. Similar results are achieved in our experiments using a sequential reactant injection approach at constant growth temperature.

Figure 1 shows TEM images of Ge-Si and Ge-Si-Si heterostructure nanorods. The naming of the nanorods represents the order of the precursor injection steps. So, Ge-Si-Si nanorods were made by three sequential injections of DPG followed by trisilane and then again, trisilane. The nanorods are reasonably uniform in diameter and length. There are spherical seed particles of Sn present on many of the nanorods and the nanorods are generally kinked. Figure 2 shows high resolution TEM data for a Ge-Si nanorod. The Ge and the Si segments are readily

6

distinguished by a strong difference in imaging contrast (Figure 2a). The transition from Ge to Si occurs sharply across a flat interface (Figure 2b-c). The strain distribution across the Ge-Si heterojunction was interrogated using geometric phase analysis (GPA) to map the lattice distortion at the interface.[53,54] Figure 2d shows the dilatation map obtained by applying the GPA algorithm to the Ge (1-11) plane, along the [1-11] axial direction of the nanowire. The difference in the *d*-spacing of the analyzed {111} planes at both sides of the heterostructure is in good agreement with pure Si and Ge relaxed segments. The theoretical, in bulk, mismatch between Si and Ge should be -4.07%, which is what is observed using GPA. The sharpness of the heterojunction in terms of lattice strain determined from the strain vs position plot shows that the transition region is about 3 nm (Figure 2e).
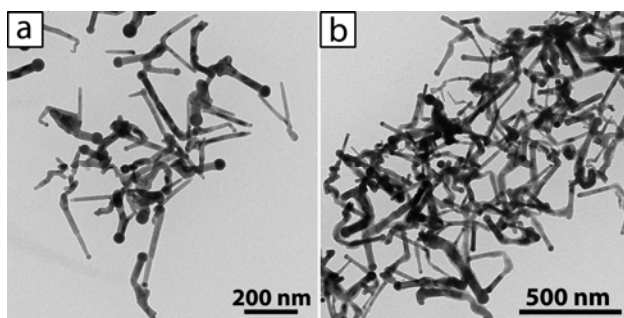
Figure 1. TEM images of a field of nanorods: (a) short Sn seeded Ge-Si nanorods and (b) Sn seeded Ge-Si-Si nanorods.
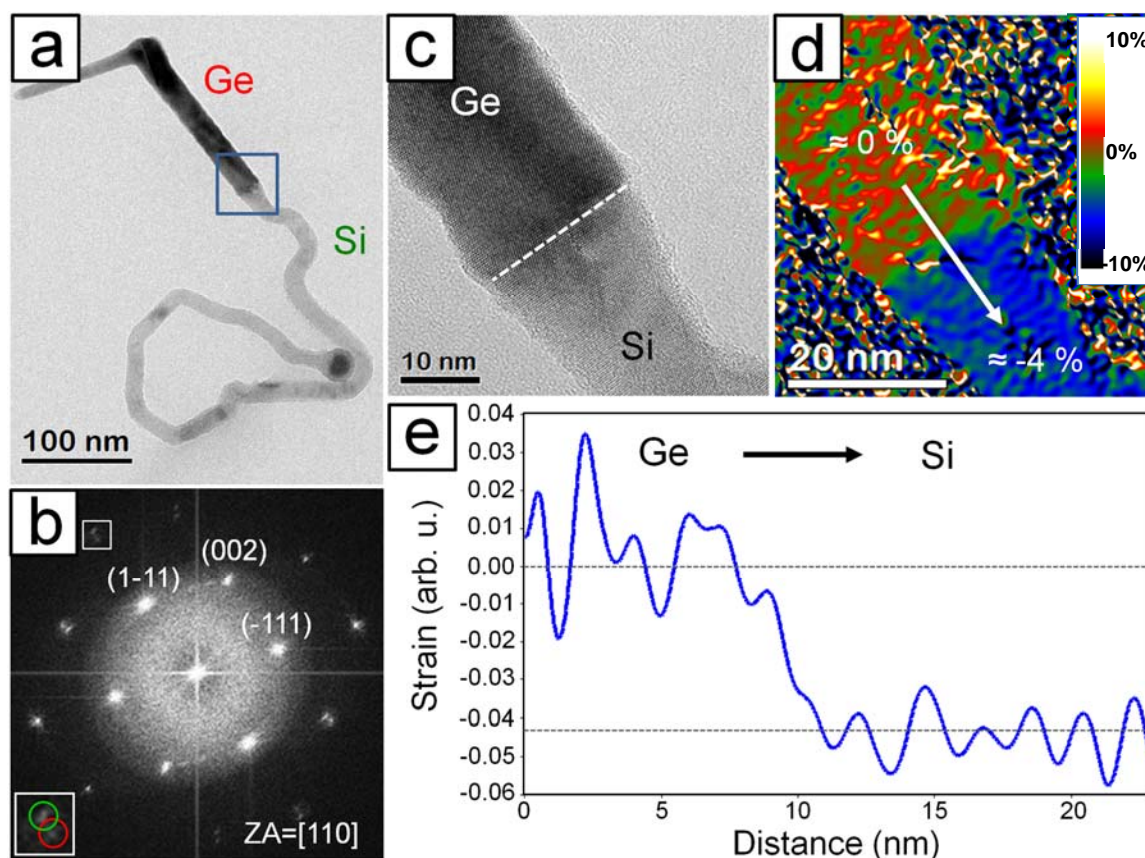
Figure 2. TEM examination of a Ge-Si heterostructure nanorod. (a) Low-resolution TEM image of a Ge-Si heterostructure nanorod. (b) The indexed FFT shows that both the Ge and the Si segments grow epitaxially along <111> direction; on the bottom left, a zoomed-in inset of the area in white box resolves two reflections corresponding to Ge (in red circle) and Si (in green circle). (c) HRTEM image of the interface region that corresponds to the area indicated by the blue box in (a). (d) Dilatation map obtained by applying GPA to the Ge (1-11) growth plane shows the Si segment with a mismatch of about -4% compared to the Ge segment, in agreement with a completely relaxed system. The false temperature color scale used is normalized between ± 10 % lattice dilatation. (e) The strain profile taken along the arrow defined in (d) corresponds to an abrupt interface (~3 nm).

The large lattice mismatch between Si and Ge leads to the formation of interfacial misfit dislocations to release the strain,[55-57] as shown by the GPA analysis and lattice-resolved HRTEM image (Figure 3a-d). A few nanometers away from the Si-Ge interface while the nanorods continue to grow in the [1-11] direction, stacking faults on a {111} plane propagating in the [1-12] direction are observed (Figures 3e, 3f and 4). Those stacking faults were found nucleated from the misfit dislocations, and either pinned to the surface (Figures 3e and 3f) or stopped by another misfit dislocation (Figure 4).[58] Both of misfit dislocations and stacking faults can be easily distinguished in the GPA mappings of the local strain, consistent with the previous finding that the normal nucleation centers are the positions of highly localized strain.[59,60]
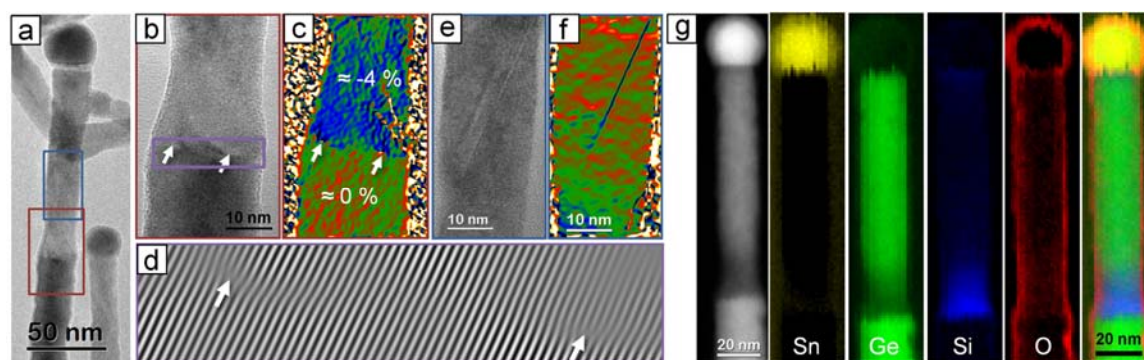

Figure 3. TEM examinations of a Ge-Si heterostructure nanorod. (a) Low-resolution TEM image of the Ge-Si heterostructure nanorod. (b) A zoomed-in HRTEM image of the interface region that corresponds to the area indicated by the red box in (a). (c) (1-1-1) GPA dilatation map of the same region in (b), showing a 4% compression of the {111} plane across the interface (both Si and Ge relaxed lattices away from the heterojunction). (d) Filtered image of the (1-1-1) plane at the interfacial region indicated by the purple box in (b). White arrows indicate the presence of misfit dislocations in (b-d). (e) A zoomed-in HRTEM image and (f) dilatation map of the Si (1-

11) plane of the region that corresponds to the area indicated by the blue box in (a) show the presence of a stacking fault. (g) ADF image and corresponding EELS mapping of the Ge-Si heterostructure nanorod. Strain maps range between -10 and +10 % lattice dilatations (same color scale bar as in Figure 2d).
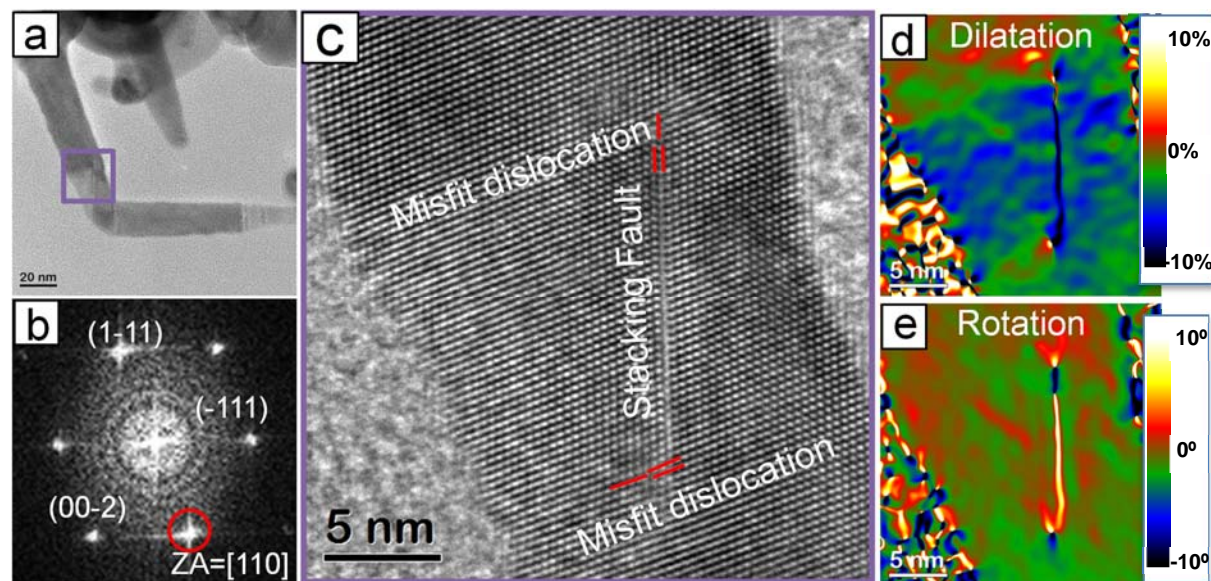
Figure 4. (a) HRTEM image of a Ge-Si-Si nanorod and (b) corresponding indexed FFT. (c) HRTEM image of the stacking fault in the Si region indicated by the purple box in (a). (d,e) GPA dilatation and rotation maps, respectively, for the (-11-1) plane. The dilatation map covers ± 10% plane deformations and the rotation ±10º.

Suppression of Si growth along the length of the nanorod. We found that as nanorod growth proceeded along the length of the Ge-Si nanorod past the heterojunction, the composition of the nanorod shifted from Si back to Ge. For example, Figure 3g shows an electron energy loss spectroscopy (EELS) analysis of the elemental composition of a Ge-Si heterostructure nanorod. The EELS mappings in Figure 3g show the presence of both a sharp Ge-Si interface as discussed

above, but also a gradual shift from Si back to Ge composition at about 20 nm away from the sharp heterojunction interface. After this transition region, the Si signal was completely diminished and the nanorod turned to pure Ge extending all the way to the Sn seed, even though no additional Ge reactant was added to the nanorod growth mixture.

This gradual change from Si back to Ge could be due to the depletion of Si reactant and a reaction of residual Ge in the system; however, this seems not to be the case. It appears that residual tetraphenyl germane—a reaction byproduct from the decomposition of DPG—reacts with trisilane to suppress Si growth and promote Ge addition to the nanorods. To verify this, two reactions were carried out: triple injections in the order of DPG-trisilane-trisilane to obtain the Ge-Si-Si nanorods, and triple injections in the order of DPG-trisilane-DPG to obtain Ge-Si-Ge nanorods.

Figure 5 shows EELS mappings of a Ge-Si-Si heterostructure nanorod and Figure 6 shows EELS mappings of a Ge-Si-Ge heterostructure nanorod. In Figure 5, the Ge-Si-Si nanorod exhibits an abrupt Ge-Si junction similar to the Ge-Si nanorod in Figure 3: after trisilane was introduced into the reaction, the nanorod composition changes immediately from Ge to Si. But at a distance of about 20 nm from the heterojunction, the Si signal begins to decrease and the Ge signal rises and eventually dominates the composition until the second injection of trisilane again led to a sharp transition from Ge to Si. The second Ge-Si junction is about 50 nm away from the initially formed heterojunction. And once again, the nanorod turns back gradually to Ge away from the second heterojunction.
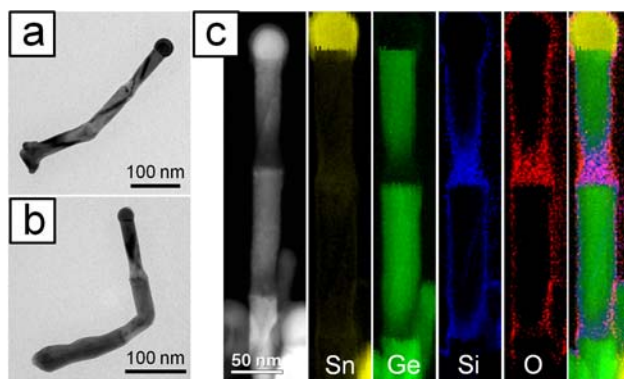
Figure 5. (a, b) Low-res TEM images of Ge-Si-Si heterostructure nanorods. (c) ADF image and

corresponding EELS mappings of the nanorod.
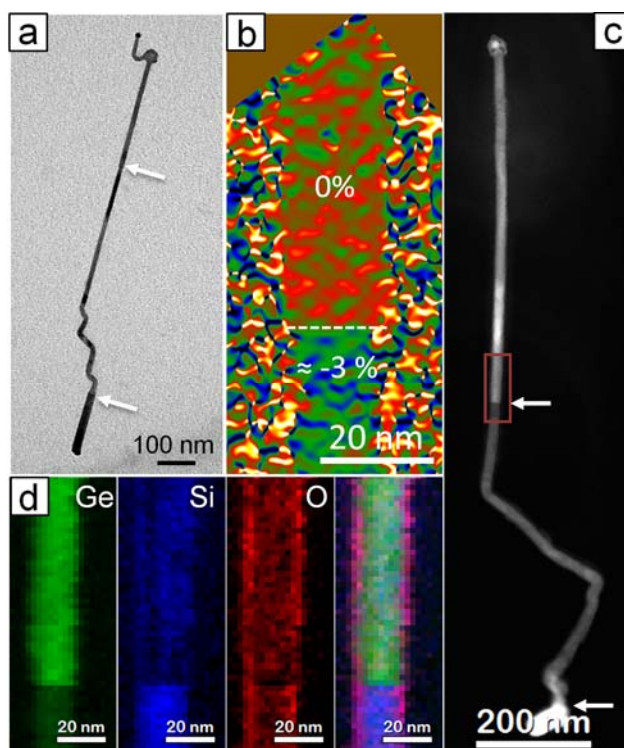
Figure 6. (a) Low-resolution TEM image of a Ge-Si-Ge heterostructure nanorod, with white

arrows indicating two Si-Ge junctions. (b) GPA Dilatation map of the region that corresponds to

the area indicated by the red box in (c), calculated using the {111} growth plane. Dilatation

normalized between ±10%. The 3% compression in the Si-rich segment instead of 4%, points to

12

a content of Ge up to 25% according to Vegard's law. It is in good agreement with the Ge

content obtained in EELS mapping in (d). (c) ADF image and (d) corresponding EELS mapping

of a Ge-Si-Ge heterostructure nanorod at the top interface.

Figure 6 shows the EELS mappings of a Ge-Si-Ge nanorod at the second interface—in

other words, the Si-Ge heterojunction created by the second injection of DPG. This particular

nanorod was grown by increasing the amount of trisilane injected from 42 μL to 63 μL to

produce a longer Si-rich segment. Away from the abrupt Ge-Si interface, the Si-rich segment is

composed of about 75% Si and 25% Ge. Once the second injection of DPG occurs, the nanorod

again becomes pure Ge. Along the length of the Ge segment formed after the second DPG

injection, some Si signal is still observed on the surface of the nanorod coexisting with O,

indicating that there is a shell of amorphous SiO_x. The introduction of Ge completely quenches

Si incorporation; whereas, trisilane injection creates an initially pure Si region, but gradually the

nanorod composition switches back to Ge. Furthermore, the EELS mappings show that the

nanorods exhibit a surface oxide and that the Si sections are more heavily oxidized than the Ge

sections.

Sn-seeded Si-Ge heterojunction nanorod reaction pathway. The use of Sn as a seed

metal for the SLS growth of the Si-Ge heterojunction nanorods helps create an abrupt Si-Ge

interface. The side reactions between the Ge and Si species in solution, however, also influence

the composition of the nanorods. Figure 7 provides an illustration of the SLS growth mechanism

of Ge-Si heterostructure nanorods using Sn seeds, DPG and trisilane reactants. There are two

primary reactions that occur: (1) the decomposition of DPG via phenyl redistribution to produce

Ge atoms that incorporate into the nanorod and tetraphenyl germane (TPG) as an *unreactive* byproduct in solution;[61] (2) the decomposition of trisilane that produces Si atoms that incorporate into the nanorods and hydrogen gas that is released as a byproduct.[62,63] TPG is unreactive at the temperatures used to make the nanorods—except in the presence of Si.[50] The phenyl groups undergo the same redistribution reaction in the presence of Si to leave Ge and bond with Si to create the more stable phenylsilane compounds.[64,65] We have observed (and utilized) this phenyl redistribution between Ge and Si species to increase the yield of Ge nanowires for example by adding phenylsilane as a phenyl sink.[50] In the synthesis of the Si-Ge heterostructure nanorods, the redistribution of phenyl groups from Ge onto Si in solution is not desirable, as it leads to a gradual transition in composition of the nanorod back to Ge after the Si initially abrupt Ge-Si interface. This side reaction competes with the reaction (2) and suppresses the production of Si atoms. Therefore, as shown in Figures 3 and 5 and illustrated in Figure 7b, Si no longer incorporates into the nanorod after the initial transient growth. This additionally verifies that the Sn seeds yield nanorods with composition that mirrors the composition of the reactant species. When TPG ends up being depleted in the solution, trisilane eventually can resume decomposition and Si can again incorporate into the nanorod (Figures 6 and 7c). In the opposite way, the presence of trisilane does not inhibit the growing of Ge but instead can accelerate DPG decomposition if anything. Therefore, Si is not incorporated after DPG injection (Figure 6).

14
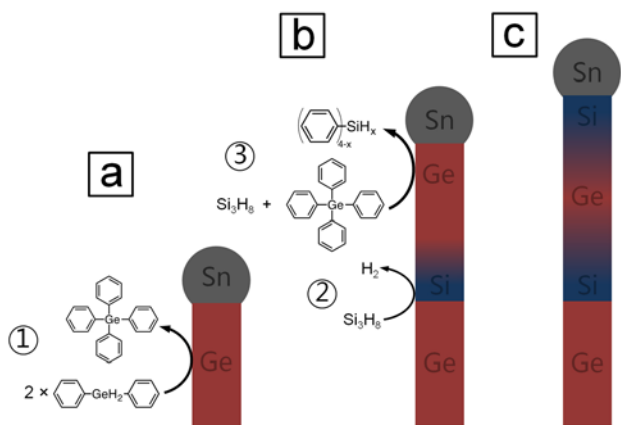
Figure 7. Illustration of the growth mechanism of Si-Ge heterostructure nanorods. (a) The decomposition of DPG produces Ge atoms and TPG. Ge atoms incorporate into the Sn and nucleate into Ge nanorods. (b) Trisilane decomposes into Si atoms that incorporate into the nanorod and form an abrupt heterojunction with Ge. However, TPG remaining in the reaction mixture reacts with trisilane to form phenyl silane, which is relatively unreactive and thus traps Si and prevents it from contributing to nanorod growth. (c) Si growth resumes after TPG is depleted.

CONCLUSIONS

Sn nanoparticles provide effective SLS seeds for Si-Ge heterostructure nanorods with abrupt interfaces. The low solubility of Si and Ge in Sn guarantees the fast reflection of the species in the reaction solution on the composition of the nanorod. Composition EELS mappings of the entire nanorods however show that the composition of the nanorods away from the heterojunctions depends strongly on the reactions occurring between Si and Ge species in the solvent. Residual phenyl germane retards the decomposition of trisilane and leads to Si-Ge alloying along the length of the nanorod; whereas, trisilane essentially enhances the decomposition of phenyl germane and relatively pure Ge segments in the nanorods are readily

15

obtained. The synthetic approach demonstrated here is convenient in that it does not require changes in temperatures and utilizes a straightforward sequential injection of reactants. The issues with the synthesis involve the control over the side reactions between Si and Ge species in the solution. The kinetic redistribution of phenyl groups between Si and Ge play the dominant role in determining the composition of the nanorods. Compositionally abrupt Si-Ge interfaces can be obtained in the nanorods, but the overall composition in the nanorods is more complex with some sections containing pure Si and Ge and Si_xGe_{1-x} alloy with changing composition. This work shows that the colloidal synthesis of Si and Ge nanomaterials has come a long way in the recent past, but it also shows that more improvement is needed in order to achieve the rigorous compositional control of Si-Ge heterostructures using gas-phase VLS methods. In this case, it appears that the key is to find effective ways to quench each growth step and trap residual byproducts so they do not influence the growth of the next segment.

Supporting Information. Additional TEM images, X-ray diffraction (XRD) and Raman spectra. This material is available free of charge via the Internet at http://pubs.acs.org.

REFERENCES

(1) Reiss, P.; Carriere, M.; Lincheneau, C.; Vaure, L.; Tamang, S. Synthesis of Semiconductor Nanocrystals, Focusing on Nontoxic and Earth-Abundant Materials. *Chem. Rev.* **2016**, *116*, 10731-10819.

(2) Boles, M. A.; Engel, M.; Talapin, D. V. Self-Assembly of Colloidal Nanocrystals: From Intricate Structures to Functional Materials. *Chem. Rev.* **2016**, *116*, 11220-11289.

(3) Wang, F.; Dong, A.; Buhro, W. E. Solution-Liquid-Solid Synthesis, Properties, and Applications of One-Dimensional Colloidal Semiconductor Nanorods and Nanowires. *Chem. Rev.* **2016**, *116*, 10888-10933.

(4) Schaak, R. E.; Emerging Strategies for the Total Synthesis of Inorganic Nanostructures. *Angew. Chem. Intl. Ed.* **2013**, *52*, 6154-6178.

(5) Cozzoli, P. D.; Pellegrino, T.; Manna, L. Synthesis, Properties and Perspectives of Hybrid Nanocrystal Structures. *Chem. Soc. Rev.* **2006**, *35*, 1195-1208.

(6) Hines, M. A.; Guyot-Sionnest, P. Synthesis and Characterization of Strongly Luminescing ZnS-Capped CdSe Nanocrystals. *J. Phys. Chem.* **1996**, *100*, 468-471.

(7) Dabbousi, B. O.; Rodriguez-Viejo, J.; Mikulec, F. V.; Heine, J. R.; Mattoussi, H. Ober, R.; Jensen, K. F.; Bawendi, M. G. (CdSe)ZnS Core-Shell Quantun Dots: Synthesis and Characterization of a Size Series of Highly Luminescent Nanocrystallites. *J. Phys. Chem. B* **1997**, *101*, 9463-9475.

(8) Eychmuller, A.; Mews, A.; Weller, H. A Quantum Dot Quantum Well: CdS/HgS/CdS. *Chem. Phys. Lett.* **1993**, *208*, 59-62.

(9) Milliron, D. J.; Hughes, S. M.; Cui, Y.; Manna, L.; Li, J.; Wang, L.-W.; Alivisatos, A. P. Colloidal Nanocrystal Heterostructures with Linear and Branched Topology. *Nature*, **2004**, *430*, 190-195.

(10) Dong, A.; Wang, F.; Daulton, T. L; Buhro, W. E. Solution-Liquid-Solid (SLS) Growth of ZnSe-ZnTe Quantum Wires having Axial Heterojunctions. *Nano Lett.* **2007**, *7*, 1308-1313.

(11) Laocharaoensuk, R.; Planiappan, K.; Smith, N. A.; Dickerson, R. M.; Werder, D. J.; Baldwin, J. K.; Hollingsworth, J. A. Flow-Based Solution-Liquid-Solid Nanowire Synthesis. *Nat. Nanotechnol.* **2013**, *8*, 660-666.

(12) Shieh, F.; Saunders, A. E.; Korgel, B. A. General Shape Control of Colloidal CdS, CdSe, CdTe Quantum Rods and Quantum Rod Heterostructures. *J. Phys. Chem. B* **2005**, *109*, 8538-8542.

(13) Robinson, r. D.; Sadtler, B.; Demchenko, D. O.; Erdonmez, C. K.; Wang, L.-W.; Alivisatos, A. P. Spontaneous Superlattice Formation in Nanorods Through Partial Cation Exchange. *Science* **2007**, *317*, 355-358.

(14) Lauhon, L. J.; Gudiksen, M. S.; Wang, D.; Lieber, C. M. Epitaxial Core-Shell and Core-Multishell Nanowire Heterostructures. *Nature* **2002**, *420*, 57–61.

(15) Gudiksen, M. S.; Lauhon, L. J.; Wang, J.; Smith, D. C.; Lieber, C. M. Growth of Nanowire Superlattice Structures for Nanoscale Photonics and Electronics. *Nature* **2002**, *415*, 617–620.

(16) Vallett, A. L.; Minassian, S.; Kaszuba, P.; Datta, S.; Redwing, J. M.; Mayer, T. S. Fabrication and Characterization of Axially Doped Silicon Nanowire Tunnel Field-Effect Transistors. *Nano Lett.* **2010**, *10*, 4813–4818.

(17) Borg, B. M.; Dick, K. A.; Ganjipour, B.; Pistol, M.-E.; Wernersson, L.-E.; Thelander, C. InAs/GaSb Heterostructure Nanowires for Tunnel Field-Effect Transistors. *Nano Lett.* **2010**, *10*, 4080–4085.

(18) Björk, M. T.; Knoch, J.; Schmid, H.; Riel, H.; Riess, W. Silicon Nanowire Tunneling Field-Effect Transistors. *Appl. Phys. Lett.* **2008**, *92*, 13–16.

(19) Hochbaum, A. I.; Yang, P. Semiconductor Nanowires for Energy Conversion. *Chem. Rev.* **2010**, *110*, 527–546.

(20) Garnett, E.; Yang, P. Light Trapping in Silicon Nanowire Solar Cells. *Nano Lett.* **2010**, *10*, 1082–1087.

(21) Tian, B.; Zheng, X.; Kempa, T. J.; Fang, Y.; Yu, N.; Yu, G.; Huang, J.; Lieber, C. M. Coaxial Silicon Nanowires as Solar Cells and Nanoelectronic Power Sources. *Nature* **2007**, *449*, 885–889.

(22) Wang, H.; Zhang, L.; Chen, Z.; Hu, J.; Li, S.; Wang, Z.; Liu, J.; Wang, X. Semiconductor Heterojunction Photocatalysts: Design, Construction, and Photocatalytic Performances. *Chem. Soc. Rev.* **2014**, *43*, 5234–5244.

(23) Zhou, H.; Qu, Y.; Zeid, T.; Duan, X. Towards Highly Efficient Photocatalysts Using Semiconductor Nanoarchitectures. *Energy Environ. Sci.* **2012**, *5*, 6732.

(24) Liu, Y.; Liu, X. H.; Nguyen, B.-M.; Yoo, J.; Sullivan, J. P.; Picraux, S. T.; Huang, J. Y.; Dayeh, S. a. Tailoring Lithiation Behavior by Interface and Bandgap Engineering at the Nanoscale. *Nano Lett.* **2013**, *13*, 4876–4883.

(25) Song, T.; Cheng, H.; Town, K.; Park, H.; Black, R. W.; Lee, S.; Park, W. Il; Huang, Y.; Rogers, J. a.; Nazar, L. F.; Paik, U. Electrochemical Properties of Si-Ge Heterostructures as an Anode Material for Lithium Ion Batteries. *Adv. Funct. Mater.* **2014**, *24*, 1458–1464.

18

(26) Yan, R.; Gargas, D.; Yang, P. Nanowire Photonics. *Nat. Photonics* **2009**, *3*, 569-576.

(27) Dou, L.; Lai, M.; Kley, C. S.; Yang, Y.; Bischak, C. G.; Zhang, D.; Eaton, S. W.; Ginsberg, N. S.; Yang, P. Spatially Resolved Multicolor CsPbX3 Nanowire Heterojunctions Via Anion Exchange. *Proc. Nat. Acad. Sci.* **2017**, *114*, 7216-7221.

(28) Heitsch, A. T.; Akhavan, V. A.; Korgel, B. A. Rapid SFLS Synthesis of Si Nanowires Using Trisilane with In Situ Alkyl-Amine Passivation. *Chem. Mater.* **2011**, *23*, 2697-2699.

(29) Wagner, R. S.; Ellis, W. C. Vapor-Liquid-Solid Mechanism of Single Crystal Growth. *Appl. Phys. Lett.* **1964**, *4*, 89–90.

(30) Schmidt, V.; Wittemann, J. V; Gösele, U. Growth, Thermodynamics, and Electrical Properties of Silicon Nanowires. *Chem. Rev.* **2010**, *110*, 361–388.

(31) Wen, C.-Y.; Reuter, M. C.; Bruley, J.; Tersoff, J.; Kodambaka, S.; Stach, E. A.; Ross, F. M. Formation of Compositionally Abrupt Axial Heterojunctions in Silicon-Germanium Nanowires. *Science* **2009**, *326*, 1247–1250.

(32) Perea, D. E.; Li, N.; Dickerson, R. M.; Misra, A.; Picraux, S. T. Controlling Heterojunction Abruptness in VLS-Grown Semiconductor Nanowires via in Situ Catalyst Alloying. *Nano Lett.* **2011**, *11*, 3117–3122.

(33) Dayeh, S. A.; Dickerson, R. M.; Picraux, S. T. Axial Bandgap Engineering in Germanium-Silicon Heterostructured Nanowires. *Appl. Phys. Lett.* **2011**, *99*, 113105.

(34) Geaney, H.; Mullane, E.; Ramasse, Q. M.; Ryan, K. M. Atomically Abrupt Silicon-Germanium Axial Heterostructure Nanowires Synthesized in a Solvent Vapor Growth System. *Nano Lett.* **2013**, *13*, 1675–1680.

(35) Dick, K. A.; Bolinsson, J.; Borg, B. M.; Johansson, J. Controlling the Abruptness of Axial Heterojunctions in III-V Nanowires: Beyond the Reservoir Effect. *Nano Lett.* **2012**, *12*, 3200-3206.

(36) Chockla, A. M.; Harris, J. T.; Korgel, B. A. Colloidal Synthesis of Germanium Nanorods. *Chem. Mater.* **2011**, *23*, 1964–1970.

(37) Li, Z.; Kornowski, A.; Myalitsin, A.; Mews, A. Formation and Function of Bismuth Nanocatalysts for the Solution-Liquid-Solid Synthesis of CdSe Nanowires. *Small* **2008**, *4*, 1698–1702.

(38) Grebinski, J. W.; Richter, K. L; Zhang, J.; Kosel, T. H.; Kuno, M. Synthesis and Characterization of Au/Bi Core/Shell Nanocrystals: A Precursor toward II-VI Nanowires. *J. Phys. Chem. B* **2004**, *108*, 9745-9751.

19

(39) Wang, F.; Buhro, W. E. An Easy Shortcut Synthesis of Size-Controlled Bismuth Nanoparticles and Their Use in the SLS Growth of High-Quality Colloidal Cadmium Selenide Quantum Wires. *Small* **2010**, *6*, 573-581.

(40) Geaney, H.; Kennedy, T.; Dickinson, C.; Mullane, E.; Singh, A.; Laffir, F.; Ryan, K. M. High Density Growth of Indium Seeded Silicon Nanowires in the Vapor Phase of a High Boiling Point Solvent. *Chem. Mater.* **2012**, *24*, 2204–2210.

(41) Mullane, E.; Kennedy, T.; Geaney, H.; Dickinson, C.; Ryan, K. M. Synthesis of Tin Catalyzed Silicon and Germanium Nanowires in a Solvent–Vapor System and Optimization of the Seed/Nanowire Interface for Dual Lithium Cycling. *Chem. Mater.* **2013**, *25*, 1816–1822.

(42) Rathi, S. J.; Jariwala, B. N.; Beach, J. D.; Stradins, P.; Taylor, P. C.; Weng, X.; Ke, Y.; Redwing, J. M.; Agarwal, S.; Collins, R. T. Tin-Catalyzed Plasma-Assisted Growth of Silicon Nanowires. *J. Phys. Chem. C* **2011**, *115*, 3833–3839.

(43) Lu, X.; Hessel, C. M.; Yu, Y.; Bogart, T. D.; Korgel, B. A. Colloidal Luminescent Silicon Nanorods. *Nano Lett.* **2013**, *13*, 3101–3105.

(44) Lu, X.; Korgel, B. A. A Single-Step Reaction for Silicon and Germanium Nanorods. *Chem. - A Eur. J.* **2014**, *20*, 5874–5879.

(45) Stolle, C. J.; Lu, X.; Yu, Y.; Schaller, R. D.; Korgel, B. A. Efficient Carrier Multiplication in Colloidal Silicon Nanorods. *Nano Lett.* **2017**, *17*, 5580-5586.

(46) Sivaram, S. V.; Hui, H. Y.; de la Mata, M.; Arbiol, J.; Filler, M. A. Surface Hydrogen Enables Subeutectic Vapor-Liquid-Solid Semiconductor Nanowire Growth. *Nano Lett.* **2016**, *16*, 6717-6723.

(47) Hui, H. Y.; de la Mata, M.; Arbiol, J.; Filler, M. A. Low-Temperature Growth of Axial Si/Ge Nanowire Heterostructures Enabled by Trisilane. *Chem. Mater.* **2017**, *29*, 3397–3402.

(48) Hong, K.-H.; Kim, J.; Lee, S.-H.; Shin, J. K. Strain-Driven Electronic Band Structure Modulation of Si Nanowires. *Nano Lett.* **2008**, *8*, 1335–1340.

(49) Pryor, C. E.; Pistol, M.-E. Band-Edge Diagrams for Strained III–V Semiconductor Quantum Wells, Wires, and Dots. *Phys. Rev. B* **2005**, *72*, 205311.

(50) Lu, X.; Harris, J. T.; Villarreal, J. E.; Chockla, A. M.; Korgel, B. A. Enhanced Nickel-Seeded Synthesis of Germanium Nanowires. *Chem. Mater.* **2013**, *25*, 2172–2177.

(51) Olesinski, R.; Abbaschian, G. The Si− Sn (Silicon− Tin) System. *Bull. Alloy Phase Diagrams* **1984**, *5*, 273–276.

(52)   Olesinski, R. W.; Abbaschian, G. J. The Ge-Sn (Germanium-Tin) System. *Bull. Alloy Phase Diagrams* **1984**, *5*, 265–271.

(53)   Hÿtch, M. J.; Snoeck, E.; Kilaas, R. Quantitative Measurement of Displacement and Strain Fields from HREM Micrographs. *Ultramicroscopy* **1998**, *74*, 131–146.

(54)   Hÿtch, M. J.; Putaux, J.-L.; Pénisson, J.-M. Measurement of the Displacement Field of Dislocations to 0.03 A by Electron Microscopy. *Nature* **2003**, *423*, 270–273.

(55)   Bessire, C. D.; Björk, M. T.; Schmid, H.; Schenk, A.; Reuter, K. B.; Riel, H. Trap-Assisted Tunneling in Si-InAs Nanowire Heterojunction Tunnel Diodes. *Nano Lett.* **2011**, *11*, 4195–4199.

(56)   Queisser, H. J.; Haller, E. E. Defects in Semiconductors: Some Fatal, Some Vital. *Science* **1998**, *281*, 945–950.

(57)   Kasper, E.; Herzog, H. J.; Kibbel, H. A One-Dimensional SiGe Superlattice Grown by UHV Epitaxy. *Appl. Phys.* **1975**, *8*, 199–205.

(58)   Biswas, S.; Singha, A.; Morris, M. a; Holmes, J. D. Inherent Control of Growth, Morphology, and Defect Formation in Germanium Nanowires. *Nano Lett.* **2012**, *12*, 5654–5663.

(59)   Dayeh, S. a.; Wang, J.; Li, N.; Huang, J. Y.; Gin, A. V.; Picraux, S. T. Growth, Defect Formation, and Morphology Control of Germanium-Silicon Semiconductor Nanowire Heterostructures. *Nano Lett.* **2011**, *11*, 4200–4206.

(60)   de la Mata, M.; Magén, C.; Caroff, P.; Arbiol, J. Atomic Scale Strain Relaxation in Axial Semiconductor III–V Nanowire Heterostructures. *Nano Lett.* **2014**, *14*, 6614–6620.

(61)   Chockla, A. M.; Korgel, B. A. Seeded Germanium Nanowire Synthesis in Solution. *J. Mater. Chem.* **2009**, *19*, 996.

(62)   Heitsch, A. T.; Fanfair, D. D.; Tuan, H.-Y.; Korgel, B. A. Solution-Liquid-Solid (SLS) Growth of Silicon Nanowires. *J. Am. Chem. Soc.* **2008**, *130*, 5436–5437.

(63)   Heitsch, A. T.; Hessel, C. M.; Akhavan, V. A.; Korgel, B. A. Colloidal Silicon Nanorod Synthesis. *Nano Lett.* **2009**, *9*, 3042-3047.

(64)   Lee, D. C.; Hanrath, T.; Korgel, B. A. The Role of Precursor-Decomposition Kinetics in Silicon Nanowire Synthesis in Organic Solvents. *Angew. Chem. Intl. Ed.* **2005**, *44*, 3573-3577.

(65)   Tuan, H.-Y.; Korgel, B. A. Importance of Solvent-Mediated Phenylsilane Decomposition Kinetics for High-Yield Solution-Phase Silicon Nanowire Synthesis. *Chem. Mater.* **2008**, *20*, 1239-1241.

21

1
2
3
4
5
6
7
8
9
10
11
12
13
14
15
16
17
18
19
20
21
22
23
24
25
26
27
28
29
30
31
32
33
34
35
36
37
38
39
40
41
42
43
44
45
46
47
48
49
50
51
52
53
54
55
56
57
58
59
60

22

1
2
3
4
5
6
7
8
9
10
11
12
13
14
15
16
17
18
19
20
21
22
23
24
25
26
27
28
29
30
31
32
33
34
35
36
37
38
39
40
41
42
43
44
45
46
47
48
49
50
51
52
53
54
55
56
57
58
59
60

For Table of Contents Use Only